Validation and Application of Hysteresis Loss Model for HTS Stacks and Conductors for Fusion Applications

Andrea Zappatore, Nikolay Bykovskiy, and Gianluca De Marzi

***Abstract*—Numerous conductor designs for pulsed magnets based on High Temperature Superconductors (HTS), featuring stacks of tapes are currently being proposed. A major contribution to the AC losses is expected to be given by hysteresis losses. Several numerical models have been developed for the computation of hysteresis losses, however the lack of experimental data in conditions relevant for the coil operation did not allow extensive validation of those models. Here, we present the AC loss tests performed on HTS conductor with transport current in conditions of partial or full field penetration. After the validation of a numerical model on those data, we analyze the losses expected during the operation of the EU DEMO CS coil, assessing possible analytical formulations for the calculation of hysteresis losses in DEMO-relevant conditions.**

***Index Terms*—AC losses, electro-magnetics, experiment, numerical modelling.**

I. Introduction

HIGH Temperature Superconductors (HTS) are currently being considered in several designs of nuclear fusion magnets [1]. Some of them are being proposed for pulsed magnets and they typically consist of stacks of HTS tapes, e.g., those proposed and manufactured by SPC (Switzerland) [2], CFS (US) [3] and ENEA (Italy) [4]. In pulsed operating conditions, heat is deposited in the conductors due to AC losses. One of the contributions to the total AC losses are the hysteretic ones, which, in HTS could play a major role with respect to other loss mechanisms, e.g., coupling losses, as shown in [5].

Large effort has been put recently in developing numerical models able to compute hysteresis losses in tapes or stacks [6]. However, only a limited number of experimental tests have been performed to quantify hysteresis losses in conditions relevant for fusion magnets. Recently, AC loss tests were performed on sub-sized HTS conductors [7], also measuring the losses in case of DC current and AC magnetic field [8].

Manuscript received 26 September 2023; revised 24 January 2024; accepted 17 February 2024. Date of publication 26 February 2024; date of current version 7 March 2024. This work was supported by European Union through Euratom Research and Training Program under Grant 101052200—EUROfusion. *(Corresponding author: Andrea Zappatore.)*

Andrea Zappatore is with NEMO group, Dipartimento Energia, Politecnico di Torino, 10124 Torino, Italy (e-mail: andrea.zappatore@polito.it).

Nikolay Bykovskiy is with Swiss Plasma Center, École Polytechnique Fédérale de Lausanne, 5232 Villigen, Switzerland (e-mail: nikolay.bykovskiy@psi.ch).

Gianluca De Marzi is with ENEA, 00044 Frascati, Italy (e-mail: gianluca.demarzi@enea.it).

Color versions of one or more figures in this article are available at https://doi.org/10.1109/TASC.2024.3369584.

Digital Object Identifier 10.1109/TASC.2024.3369584

The aim of the present work is first to validate a numerical model for the calculation of hysteresis losses in a stack of tapes and then to apply it to quantify the losses expected during the operation of the EU DEMO hybrid Central Solenoid (CS) [9], proposing also a possible analytical formulation which would ease the calculation during both the conductor design as well as for detailed studies, e.g., thermal-hydraulic analyses [10], [11], [12] which receives as input the power deposition due to AC losses.

The paper is structured in the following way: first, the numerical model and the experimental tests are described, then the comparison between the numerical and experimental results is discussed. The last section is devoted to the CS-relevant computation of the losses throughout its current scenario and to the comparison with possible analytical formulations.

II. Experimental Tests

AC loss tests were performed in SULTAN [8] in the framework of the Quench Experiment campaign launched by EUROfusion in 2020, see [7] and [13]. The tests were carried out applying a sinusoidal AC external field of ± 0.2 T with a frequency of 0.3 Hz up to 1.5 Hz, on top of a DC background field. In case of 0 T and 2 T background field, no transport current was applied; in case of 6 T and 9 T background field, 15 kA DC current was supplied to the sample. In Fig. 1, the AC losses measured for the BSCCO conductor are reported. The BSCCO conductor is composed by a triplet of stacks enclosed in a copper profile and twisted together, see [7] for more details. They were quantified through calorimetric assessment using the sensors which measured the supercritical He flow temperature before and after the AC field region, together with a mass flow meter at the inlet of the conductor. The BSCCO conductor was chosen because it presented larger hysteresis losses, thus more easy to quantify, than the REBCO conductor.

III. Numerical Model

Here the description of the 2D model, implemented in COMSOL [14], is reported. The geometrical parameters considered in the simulations are reported in Table I. The cross-section of the stack is simulated together with a circular air domain with radius ten times larger than the height of the stack.

The governing equation of the model is reported in (1). It directly comes from the combination of the Ampere's and Faraday's law [15]:

$$\mu_0 \frac{\partial \boldsymbol{H}}{\partial t} + \nabla \times (\rho \nabla \times \boldsymbol{H}) = 0 \tag{1}$$

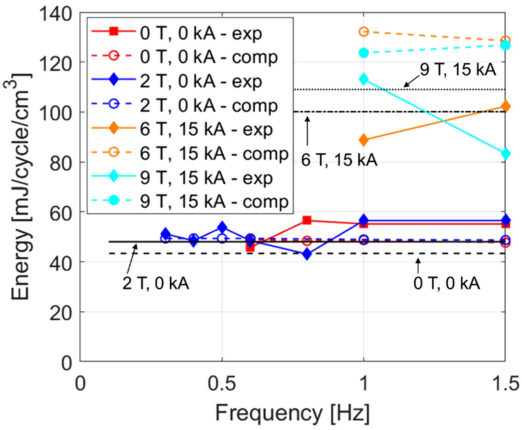

Fig. 1 Measured AC losses per unit volume of stack per cycle compared with hysteresis losses computed with the numerical model and analytical formulae (indicated by the arrows).

TABLE I
GEOMETRICAL DIMENSIONS OF TAPES AND STACK

Parameter	Value
Number of tapes	19
Width of the tape and stack [mm]	4.30
Height of the tape [mm]	0.23
Height of the stack [mm]	4.37

TABLE II
PARAMETERS OF THE SCALING LAW OF THE SUPERCONDUCTOR

Parameter	Value
n	34
A [A/m^2]	$9.2738 \cdot 10^{10}$
T_c [K]	110
T_0 [K]	14
B_0 [T]	54.94
α	0.8933

Where μ_0 is the vacuum permeability, **H** is the magnetic field intensity (with components H_x and H_y, the model being 2-dimensional) and ρ is the electric resistivity. The latter is computed according to the power law in the stack domain and it is set to a large value (1 Ω·m) in the air domain. The electric resistivity in the stack region is given by:

$$\rho = \frac{E_C}{J_C\left(B,T\right)} \cdot \left(\frac{J}{J_C\left(B,T\right)}\right)^{n-1} \tag{2}$$

Where E_C is the critical field ($=$ 10^{-4} V/m), $J_C(B,T)$ is the scaling law for the BSCCO reported in (3) with the corresponding parameters reported in Table II (the temperature is assumed constant and equal to 6 K), J is the current density, computed as $J = \frac{\partial H_y}{\partial x} - \frac{\partial H_x}{\partial y}$ and n is the n-value of the power law.

$$B_{irr} = B_0 \cdot e^{-T/T0}$$
$$J_C\left(B,T\right) = A \cdot \left(1 - \frac{T}{Tc}\right)^{\alpha} \cdot e^{-B/B_{irr}} \tag{3}$$

The critical current is homogenized according to the fraction of superconducting area present in the stack, i.e., $J_{C,homogenized} = J_C(B) \cdot \frac{n_{tapes} \cdot t_{tape}}{t_{stack}}$ [16], where n_{tapes} is the number of tapes, t_{tape} is the thickness of the tape equal to 0.23 mm (the thickness of the superconducting layer is assumed equal to 0.1 mm), t_{stack} is the thickness of the stack. This allows meshing the entire stack with much less elements as the homogenization allows tackling the high aspect ratio of the HTS tapes.

The time-dependent boundary condition of the model are the components of the magnetic field intensity H_x and H_y, which are imposed on the outer edge of the air domain, whose value is that used in the analyzed test (0, 2, 6, 9 T). All the simulations are carried out considering the background field perpendicular to the tapes of the stack. The initial condition is zero-field imposed in the entire computational domain. The background magnetic field and the transport current (if present) are ramped to the rated value before the beginning of the cycle. After that, a cycle of ±0.2 T is started, in which the power deposition per unit length due to hysteresis losses is computed according to (4)

$$Q = \int_{1/(2f)}^{1/f} \int_S J \cdot E dS\, dt\, [W/m] \tag{4}$$

where f is the frequency of the cycle, S is the cross-section of the stack, E is the electric field, computed in the model as $E = \rho \cdot J$.

The transport current I_t is imposed through integral constraint on the stack according to (5)

$$I_t = \int_S J dS \tag{5}$$

The speed of computation of the model is strongly affected by the presence of transport current. If both the background field and transport current are ramped to reach the pre-cycle conditions, then the convergence of each time step is slower with respect to the case when one of the two variables is time-varying and the other is kept constant. Therefore, in the simulations, the magnetic field is first ramped to the rated value and a plateau is simulated in order to reach equilibrium before starting the cycle. If current is present, then it is ramped after the magnetic field. Even with this strategy, the numerical convergence becomes very slow (up to twenty-times slower than the case without transport current) when the transport current reaches 95 % of the critical current.

As the electromagnetic interaction of the stacks is low, we opted to simulate only one stack. Furthermore, to account for the presence of the twisting in the experiment with a 2D numerical model, the obtained power deposition is multiplied by a factor $2/\pi$, as derived in [17], before comparing the results with the experimental data.

IV. VALIDATION ON CONDUCTOR EXPERIMENTAL DATA

The energy per cycle computed with the numerical model is compared with the measured one in Fig. 1.

The results agree well both in case of absence or presence of transport current. The computed results are only mildly dependent on the frequency, as expected from the purely hysteretic nature of the losses simulated in the model.

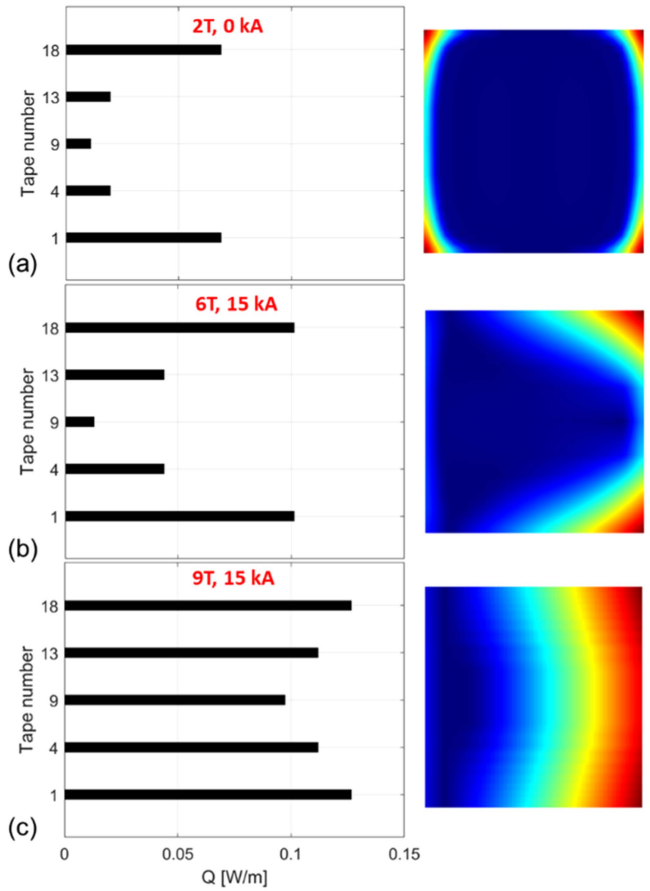

Fig. 2 Computed volumetric heat generation (normalized) with the numerical model (right) and losses in selected tapes (left) for cases (a) 2 T, 0 kA; (b) 6 T, 15 kA; (c) 9 T, 15 kA.

At 0 T and 2 T, the penetration field of the stack, which can be approximated as [2]

$$B_p = \frac{\mu_0 J_{c,e} w}{2} \tag{6}$$

where $J_{C,e} = I_{C,stack}/S$ and w is the width of the stack, is $B_p = 0.98$ T (at $B_{ext} = 2$ T), therefore an applied (varying) field of 0.2 T is not able to fully penetrate the stack. This means that the losses measured (or computed) in this condition are not representative of the actual operation condition of the full-scale conductor in a coil for fusion applications, where the background field reaches values much larger than typical B_p. The small penetration of the field is confirmed by the map of volumetric heat power reported in Fig. 2(a), together with the corresponding losses per tape reported in the bar plot. It is clear that only the top and bottom tapes are penetrated, leading to appreciable hysteresis losses mainly there. On the other hand, the rest of the stack is shielded, thus only marginally contribute to the power deposition.

In case of DC transport current, the relevant threshold for magnetic field full penetration becomes $B_p \cdot (1 - i)$ [18] (p. 430), where $i = I_t/I_C$. In the case 6 T, 15 kA, $B_p \cdot (1 - i) = 0.16$T, while in the case 9 T, 15 kA, $B_p \cdot (1 - i) = 0.09$ T, therefore, in the latter case, the stack is expected to be fully penetrated, while the former is in a transition regime between the two extreme cases.

Fig. 2(b) and (c) show that the stack can be effectively fully penetrated even with a background field oscillating with an amplitude of 0.2 T. In the case 6 T, 15 kA, the central part of the stack is still shielded, however the stack is clearly more penetrated than the 2 T, 0 kA case. A negligible effect of shielding is visible at 9 T, 15 kA, where all the tapes are rather uniformly contributing to the total losses. Note that the asymmetry in the map of the volumetric heat deposition is due to the presence of the transport current, which alters the symmetry even if the external magnetic field is symmetric, as demonstrated in [18] p. 430.

Analytical formulae developed for magnetization losses in rectangular bars [19] and for hysteresis losses in a superconducting slab with transport current [20] are also compared with the experimental results. The formulae proposed in [20], although in principle developed only for the coil charge, are useful also because they account the time derivative of the external magnetic field and of the current, which means that they can be used also in case the power deposition is of interest rather than just energy per cycle. This is the case when the power deposition is of interest, such as during the current scenario foreseen for the EU DEMO CS coils, as it is the driver of the conductor temperature evolution, which in turn determines the temperature margin.

V. Losses During EU DEMO CS Current Scenario

Hysteresis losses during the current scenario foreseen in the hybrid option of the EU DEMO CS were computed with both the validated numerical model as well as with the available formulae and they are discussed in this section. The model is that described in Section III and the losses discussed here are for a single stack in the innermost layer (largest magnetic field) of the central module of the CS. To reach the critical current which satisfies the design requirement for the minimum current sharing temperature (= 8.2 K), there would be 11 stacks made as those simulated in the numerical model.

The current scenario foreseen in the EU DEMO CS is composed by different phases: a charge phase to bring the coil at nominal current and magnetic field, a breakdown (BD) phase where there is a strong magnetic field variation in a short time (0.75 T in 0.8 s), a plasma current ramp up phase (PCRU) where there is a decrease in the magnetic field of the CS from 15 T down to −2.5 T, a plasma burn phase where there is a slow linear decrease of the magnetic field down to −15 T and a discharge phase when the coil is brought to zero current before starting a new cycle. Note that the perturbations to the magnetic field coming from feed-back systems, plasma motion and so on are not considered in this analysis.

In Fig. 3, we report the hysteresis losses computed in the different phases of the scenario, comparing the computed results with different analytical formulae:

- during the charge phase, see Fig. 3(a), after the applied external magnetic field (B_a) has overcome the penetration field ($B_p = 0.8$ T), the stack can be approximated as a slab, which is confirmed by the very good agreement between the results computed numerically and those obtained with the analytical formulae. When $B_a < B_p$, the finite shape of the stack has a non-negligible impact on the losses, as confirmed by the agreement between the analytical formulae for a square stack [19] and the computed results. In this interval, the losses would be underestimated by the analytical formulae for a non-saturated slab [20] up to a factor 3.

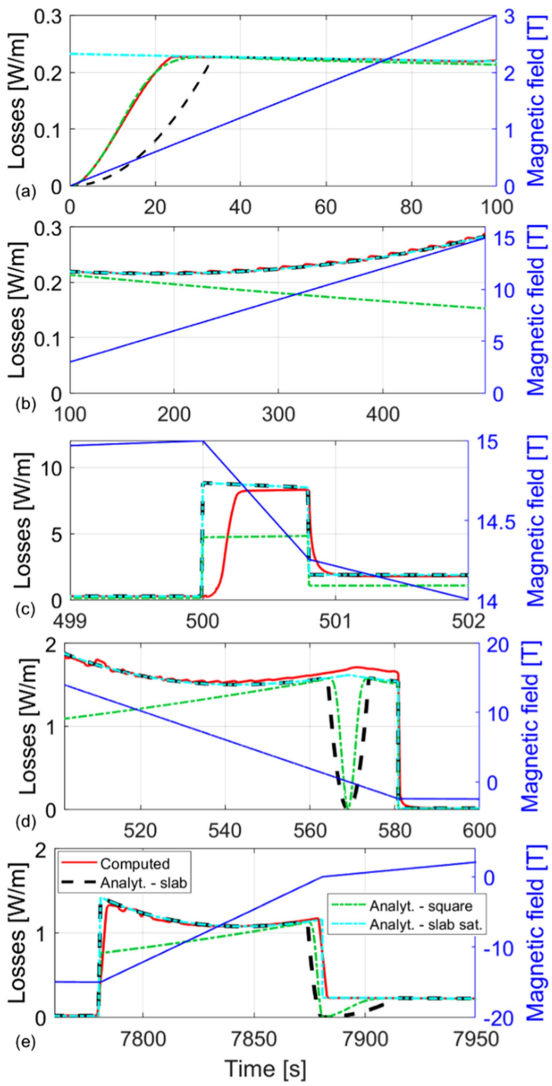

Fig. 3. Evolution of the hysteresis losses computed with the numerical model and different analytical formulae during (a) the first and (b) second part of the initial charge, (c) the breakdown, (d) the plasma current ramp up, and (e) the zero-crossing during the discharge and the new charge.

- during the second part of the charge phase, see Fig. 3(b), the analytical formulation for a current-carrying slab [20] agrees with the numerical results. On the other hand, the analytical formulation for a square stack does not account for the presence of the transport current and this leads to an underestimation of the losses in this interval, if computed with this formulation.
- during the breakdown phase, see Fig. 3(c), the analytical formulae are not able to correctly account for the screening of the stack which reacts with a delay (losses are generated first at the four angles of the stack) of the order of 0.1 s, as shown by the numerically computed results. This leads the formulae to overestimate the losses for that time interval, while they agree well once the losses become steady as consequence of a steady variation in time of magnetic field and current. This phase is particularly critical in terms of temperature margin as the conductor is close to its maximum current and field and a strong heat deposition is present due to the fast variation of field and current. Therefore, in this phase would be preferable to use the computed results for a more accurate estimate of the temperature margin, while the analytical formulae could anyway be used keeping in mind that they would provide a conservative result.
- during the PCRU, see Fig. 3(d), the magnetic field as well as the current cross zero, which implies zero losses if computed with the analytical formulae. However, it would be an underestimation, as part of the magnetic field is still trapped into the stack, thus this leads to losses even if the external magnetic field is zero in that instant. A possible, simple, modification to the analytical formulae for the slab with transport current would be to consider the slab fully penetrated also in this phase (see the cyan curve in Fig. 3(d)), which leads to a better agreement with the validated numerical model. An independent confirmation of the non-zero losses in case of zero-crossing comes from the formula in [21], which agree well with the computed results (not shown). In the central module, integrating over the HTS layers, a value of 2.8 kW is found, which would sum up to the 5.3 kW given by all the LTS layers.
- During plasma burn, heat deposition is low (< 0.02 W/m) and the numerical model and analytical formulae for a current-carrying slab agree very well. During the discharge-(re)charge phase, see Fig. 3(e), the set of results are compared together. During the discharge, i.e., ramp of the magnetic field from -15 T to 0 T, the losses are underestimated if the transport current is not taken into account. In the zero-crossing region, it is confirmed that the assumption of full penetrated slab reproduces better the losses than other formulae.

Therefore, the validated numerical model allows to propose a simplified formula (7) for the computation of the hysteresis losses during the current scenario of the EU DEMO CS coil. Neglecting the first ramp of a series of cycles, which is of limited interest since the nominal operation is foreseen to be periodic, the analytical formulae for a slab with transport current in the full penetrated regime [20] is accurate (or conservative in case of fast variation, such as during the BD phase), and it is here reported for convenience:

$$Q'_{hyst} = \frac{B_p^2}{2\mu_0}\left(\frac{\left|\dot{B}\right|}{B_p} + \frac{I_t^2}{I_C^2}\frac{\left|\dot{B}\right|}{B_p} + 2\frac{|I_t|}{I_C}\frac{\left|\dot{I}_t\right|}{I_C}\right)\cdot S \qquad (7)$$

where $\dot{B}$ and $\dot{I}_t$ are the time derivative of the external magnetic field and of the transport current in the stack.

VI. Conclusion

AC loss tests performed on a BSCCO conductor in conditions relevant for fusion coils were used to successfully validate a numerical model for the computation of hysteresis losses. The model was used to compute the hysteresis losses during the current scenario foreseen in the EU DEMO CS coil, proposing an analytical formulation for their computation.

Acknowledgment

Views and opinions expressed are however those of the author(s) only and do not necessarily reflect those of the European Union or the European Commission. Neither the European Union nor the European Commission can be held responsible for them.

REFERENCES

[1] N. Mitchell et al., "Superconductors for fusion: A roadmap," *Supercond. Sci. Technol.*, vol. 34, Sep. 2021, Art. no. 103001.

[2] D. Uglietti, N. Bykovsky, K. Sedlak, B. Stepanov, R. Wesche, and P. Bruzzone, "Test of 60 ka coated conductor cable prototypes for fusion magnets," *Supercond. Sci. Technol.*, vol. 28, Nov. 2015, Art. no. 124005.

[3] Z. S. Hartwig et al., "Viper: An industrially scalable high-current high-temperature superconductor cable," *Supercond. Sci. Technol.*, vol. 33, Oct. 2020, Art. no. 11LT01.

[4] L. Muzzi et al., "Design and feasibility assessment of an HTS sector shaped high-current conductor for fusion coils," *IEEE Trans. Appl. Supercond.*, vol. 33, no. 5, Aug. 2023, Art. no. 4200106.

[5] D. Uglietti, R. Kang, R. Wesche, and F. Grilli, "Non-twisted stacks of coated conductors for magnets: Analysis of inductance and AC losses," *Cryogenics*, vol. 110, 2020, Art. no. 103118.

[6] F. Grilli, E. Pardo, A. Stenvall, D. N. Nguyen, W. Yuan, and F. Gomory, "Computation of losses in HTS under the action of varying magnetic fields and currents," *IEEE Trans. Appl. Supercond.*, vol. 24, no. 1, Feb. 2014, Art. no. 8200433.

[7] O. Dicuonzo et al., "Upgrade and commissioning of the SULTAN facility to host quench experiments on HTS high current conductors," *IEEE Trans. Appl. Supercond.*, vol. 31, no. 5, Aug. 2021, Art. no. 9500505.

[8] N. Bykovskiy, H. Bajas, O. Dicuonzo, P. Bruzzone, and K. Sedlak, "Experimental study of stability, quench propagation and detection methods on 15 kA sub-scale HTS fusion conductors in SULTAN," *Supercond. Sci. Technol.*, vol. 36, Feb. 2023, Art. no. 034002.

[9] R. Wesche et al., "Hybrid HTS-Nb3Sn-NbTi DEMO CS coil design optimized for maximum magnetic flux generation," *Fusion Eng. Des.*, vol. 146, pp. 10–13, 2019.

[10] A. Zappatore, G. D. Marzi, and D. Uglietti, "Impact of hysteresis losses in hybrid (HTS-LTS) coils for fusion applications," *IEEE Access*, vol. 11, pp. 100465–100478, 2023.

[11] M. Bagnasco, D. Bessette, L. Bottura, C. Marinucci, and C. Rosso, "Progress in the integrated simulation of thermal-hydraulic operation of the ITER magnet system," *IEEE Trans. Appl. Supercond.*, vol. 20, no. 3, pp. 411–414, Jun. 2010, doi: 10.1109/TASC.2010.2043836.

[12] L. Cavallucci, F. Gauthier, M. Breschi, C. Hoa, P. Bauer, and A. Vostner, "Multiphysics model of quench for the ITER Central solenoid," *IEEE Trans. Appl. Supercond.*, vol. 33, no. 5, Aug. 2023, Art. no. 4700505, doi: 10.1109/TASC.2023.3244769.

[13] A. Zappatore et al., "Quench experiments on sub-size HTS Cable-In-conduit conductors for fusion applications: Data analysis and model validation," *Cryogenics*, vol. 132, 2023, Art. no. 103695.

[14] COMSOL AB, "COMSOL Multiphysics 5.6," 2021. Accessed: Aug. 18, 2023. [Online]. Available: www.comsol.com

[15] B. Shen, F. Grilli, and T. Coombs, "Review of the AC loss computation for HTS using H formulation," *Supercond. Sci. Technol.*, vol. 33, Feb. 2020, Art. no. 033002.

[16] V. M. R. Zermeno, A. Abrahamsen, N. Mijatovic, B. Jensen, and M. P. Sørensen, "Calculation of alternating current losses in stacks and coils made of second generation high temperature superconducting tapes for large scale applications," *J. Appl. Phys.*, vol. 114, no. 17, 2013, Art. no. 173901.

[17] M. Takayasu, L. Chiesa, L. Bromberg, and J. V. Minervini, "HTS twisted stacked-tape cable conductor," *Supercond. Sci. Technol.*, vol. 25, Dec. 2011, Art. no. 014011.

[18] Y. Iwasa, *Case Study in Superconducting Magnet Design*. NY, USA: Springer, 2009.

[19] E. Pardo, D.-X. Chen, A. Sanchez, and C. Navau, "The transverse critical-state susceptibility of rectangular bars," *Supercond. Sci. Technol.*, vol. 17, pp. 537–544, Feb. 2004.

[20] S. Awaji et al., "AC losses of an HTS insert in a 25-T cryogen-free superconducting magnet," *IEEE Trans. Appl. Supercond.*, vol. 25, no. 3, Nov. 2014, Art. no. 4601405.

[21] A. Macchiagodena, M. Breschi, D. Buonafine, G. De Marzi, and L. Savoldi, "Analytical modeling of magnetization losses in twisted stacked HTS conductors," *IEEE Trans. Appl. Supercond.*, vol. 33, no. 5, Aug. 2023, Art. no. 5900705.

Open Access funding provided by 'Politecnico di Torino' within the CRUI CARE Agreement